arXiv:1612.07576v1 [cond-mat.str-el] 22 Dec 2016

Excitonic magnetism in d^6 perovskites

J. Fernandez Afonso and J. Kuneš*
Institute of Solid State Physics, TU Wien, Wiedner Hauptstr. 8, 1040 Wien, Austria and
Institute of Physics, Academy of Sciences of the Czech Republic,
Cukrovarnická 10, Praha 6, 162 53, Czech Republic
(Dated: December 23, 2016)

We use the LDA+U method to study the possibility of exciton condensation in perovskites of transition metals with d^6 electronic configuration such as $LaCoO_3$. For realistic interaction parameters we find several distinct solutions exhibiting spin-triplet exciton condensate, which gives rise to a local spin density distribution while the ordered moments are vanishingly small. Rhombohedral distortion from the ideal cubic structure suppresses the ordered state, contrary to the spin-orbit coupling which enhances the excitonic condensation energy. We explain the trends observed in the numerical simulations with the help of a simplified strong-coupling model. Our results indicate that $LaCoO_3$ is close to the excitonic instability and suggest ways to make it order.

I. INTRODUCTION

Spontaneous symmetry breaking leading to a long-range order (LRO) is a ubiquitous phenomenon in correlated materials built from atoms with degenerate ground states. For lighter elements this typically amounts to spin ordering driven by isotropic exchange or orbital ordering with anisotropic exchange. For heavier elements the spin-orbit coupling forms tightly bound spin-orbitals and thus gives rise to generally anisotropic exchange.

LRO in materials with singlet atomic ground states is rare. If the energy of an atomic excitaton is comparable to the amplitude to propagate it to neighbouring atoms spontaneous symmetry breaking may take place. LRO of this type called excitonic magnet has been studied in simple lattice models[1–6] and proposed to take place in $4d^4$ materials such as Ca_2RuO_4[1,7] or $3d^6$ cubic materials such as the $LaCoO_3$ family[3]. Here we focus on the latter.

Although no thermally driven phase transition has been observed in $LaCoO_3$, a proximity to an ordering instability or short range correlations have been discussed for a long time. The most studied proposals include the spin state ordering,[8–10] cooperative Jahn-Teller effect[11,12] and magnetic correlations.[13,14] These states can be viewed as a classical LRO of atomic states/multiplets and are generally expected to be accompanied by Co-O bond length disproportionation. Despite experimental effort the Co-O bond length disproportionation remains controversial.[15–18] Recently, high magnetic field experiments revealed a meta-magnetic transition with a peculiar temperature dependence.[19–21] Field-induced exciton condensation was suggested as an explanation[21,22] and studied in a simplified two-orbital Hubbard model by means of an effective strong coupling model[27,28] and the dynamical mean-field theory.[22] Exciton condensation was also proposed[3] to explain the phase transition observed in the $Pr_{0.5}Ca_{0.5}CoO_3$ family.[23–26]

Unlike the LROs discussed above, exciton condensation, which involves a spontaneous coherence between different atomic multiplets on the same ion, does not have a classical analog. Real materials add another dimension to the problem - the orbital degeneracy, which further expands the already rich universe of excitonic phases. In this article we investigate the excitonic magnetism in prototypical $3d^6$ perovskite by means of the mean-field LDA+U approach,[29] which makes the problem computationally feasible. The method is too simple to capture quantum or thermal fluctuations and thus cannot be used to study the transition to the condensed phase. On the other hand, it can capture the exciton condensate and thus allows us to answer the following basic questions. Are there ordered solutions at all and how does their stability depend on the strength of the onsite Coulomb interaction? Which of the many possible excitonic states has the lowest energy and why? How do the ordered solutions respond to the lattice distortions and inclusion of the spin-orbit coupling (SOC)?

The paper is organized follows. In section II we introduce the multi-component order parameter describing the exciton condensate and summarize the computational parameters used in this study. In sec-

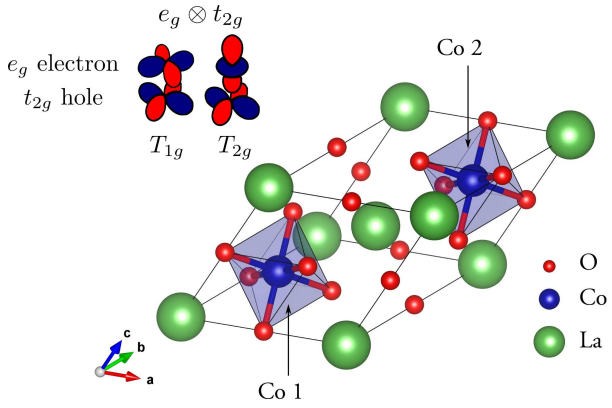

FIG. 1: The unit cell used in the calculations. In the upper left corner we show the orbital structure of the T_{1g} and T_{2g} excitons.

tion III we present the obtained ordered solutions. We have performed extensive calculations for the hypothetical cubic systems without SOC varying the interaction parameters and initial conditions. Subsequently, we investigate the effect of the rhombohedral distortion, present in the real $LaCoO_3$ structure, and SOC for a selected set interaction parameters. The main features of our numerical results are summarised in section IV. We introduce two strong-coupling models with different degree of simplification, which allow us to present semi-quantitative explanations of the observed trends. The key observations are them summarised in the compact form in section V.

II. COMPUTATIONAL METHOD

The calculations reported here were performed in the framework of the density functional theory using the LDA+U approach,[29] with the 'U' interaction in the $3d$ shell of Co and the double-counting correction corresponding to so called fully localized limit.[30] The spin polarization entered only the orbitally dependent potential acting on the $3d$ states of Co while the LDA exchange-correlation potential was not spin polarized. The calculations were done with the Wien2k[31] software. In all cases we used the unit cell of Fig. 1, which can accommodate the real $LaCoO_3$ as well as the staggered excitonic order, which was found to have lower total energy than a uniform one. No orbital or spin point symmetry was assumed.

Several crystal structures were used in this study: hypothetical cubic perovskite structure with a=3.8498 Å, the experimental $LaCoO_3$[36] and a series of structures interpolating between the two. The calculations were performed with the $10 \times 10 \times 10$ k-mesh in the full Brillouin zone, muffin-tin radii (in bohr): 2.5 for La, 1.99 for Co and 1.92 for O, and the plane wave cut-off $R_{mt}K_{max} = 6$. The Co $3d$ occupation matrices discussed in the following are expressed in the local orbital and spin coordinates tied to the CoO_6 octahedra–axes pointing (approximately) along the Co-O bonds.[37]

A. Excitonic order parameter

Although the present method is a fermionic mean-field theory, we find it instructive to refer to the strong-coupling limit of the present problem, which can be formulated in terms of hard-core bosons.[32,33] The lattice occupied by atoms in the low-spin state can then be viewed as the bosonic vacuum. A bosonic condensate is, in general, a superposition of the vacuum with some other bosonic states. We consider a wave function of the condensed system in the form of a product over Co sites

$$|\Psi\rangle = \prod_k \left(s_k \left|LS\right\rangle_k + \xi_k^\alpha \left|IS_\alpha\right\rangle_k + \zeta_k^\beta \left|HS_\beta\right\rangle_k \right). \quad (1)$$

Here, we have a superposition of the low-spin (LS, S=0), intermediate-spin (IS, S=1) and high-spin (HS, S=2) states on each Co site. Evaluating the local occupation matrix in the d-shell of Co in the above state, anomalous matrix elements, violating the cubic and spin-rotational symmetry, appear. These terms will serve as our order parameter.

We consider only IS states of the T_{1g} symmetry which correspond to the $d_{x^2-y^2} \otimes d_{xy}$, $d_{z^2-x^2} \otimes d_{xz}$ and $d_{y^2-z^2} \otimes d_{yz}$ electron-hole excitations (excitons) of the LS state. Only such excitons have sizeable amplitudes to propagate as composite objects and to condense.[22]. This assumption will be justified *a posteriori* by unrestricted calculations, which show that the order parameter has indeed the T_{1g} orbital symmetry. The anomalous elements of the Co-$3d$ occupation matrix can be described by 18 Hermitean

operators

$$\hat{O}'_{\alpha\beta} = \frac{1}{4}\sum_{i,i'=1}^{5}\sum_{\sigma\sigma'=\uparrow,\downarrow}(\Gamma'_\alpha)_{ii'}(\tau_\beta)_{\sigma\sigma'}\hat{c}^\dagger_{i\sigma}\hat{c}_{i'\sigma'}$$
$$\hat{O}''_{\alpha\beta} = \frac{1}{4}\sum_{i,i'=1}^{5}\sum_{\sigma\sigma'=\uparrow,\downarrow}(\Gamma''_\alpha)_{ii'}(\tau_\beta)_{\sigma\sigma'}\hat{c}^\dagger_{i\sigma}\hat{c}_{i'\sigma'}. \quad (2)$$

Here $\hat{c}^\dagger_{i\sigma}$ ($\hat{c}_{i\sigma}$) are the creation (annihilation) operators for an electron in the Co $3d$ state with orbital and spin indices i and σ acting on the same atom. (The site indices are not shown for sake of simplicity). The Pauli matrices τ_β ($\beta = x, y, z$) capture the spin-triplet character of the excitonic order while the 5×5 Γ_α ($\alpha = \hat{x}, \hat{y}, \hat{z}$) matrices describe the orbital structure. The primed and unprimed Γ_α matrice correspond to the symmetric (density-like) and antisymmetric (current-like) combinations respectively. The explicit form of Γ_α in cubic harmonics as well as spherical harmonics bases can be found in the Appendix.

We define the order parameter $\phi_{\alpha\beta}$ as a complex 3×3 matrix formed by the expectation values of the operators $\hat{O}'_{\alpha\beta}$ and $\hat{O}''_{\alpha\beta}$

$$\phi_{\alpha\beta} = \langle\hat{O}'_{\alpha\beta}\rangle + i\langle\hat{O}''_{\alpha\beta}\rangle = \phi'_{\alpha\beta} + i\phi''_{\alpha\beta}. \quad (3)$$

The columns $\boldsymbol{\phi}$ transform as a pseudovectors (T_{1g} representation) under the O_h point group. The rows of $\boldsymbol{\phi}$ transform as a vectors ($S = 1$ representation) under the $SU(2)$ spin rotations. We further define the norm $|\boldsymbol{\phi}| = \sqrt{\sum_{\alpha\beta}|\phi_{\alpha\beta}|^2}$ and introduce a special variable for the spin(row)-vectors $\boldsymbol{\eta}_\alpha$ ($\alpha = \hat{x}, \hat{y}, \hat{z}$), $(\boldsymbol{\eta}_\alpha)_\beta = \phi_{\alpha\beta}$.

Our choice of the order parameter can be tested *a posteriori* by comparing the calculated occupation matrices with the expected form of the anomalous part:

$$\langle\hat{c}^\dagger_{i\sigma}\hat{c}_{i'\sigma'}\rangle_A = \phi'_{\alpha\beta}(\Gamma'_\alpha)^*_{ii'}(\tau_\beta)^*_{\sigma\sigma'} + \phi''_{\alpha\beta}(\Gamma''_\alpha)^*_{ii'}(\tau_\beta)^*_{\sigma\sigma'}. \quad (4)$$

III. RESULTS

We start our presentation with idealized cubic structure without SOC, which possesses the exact O_h site symmetry and $SU(2)$ spin rotational symmetry, and proceed by continuously switching the rhombohedral distortion and adding the spin-orbit coupling.

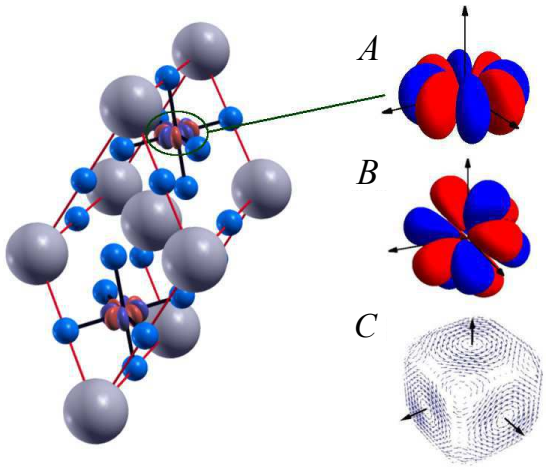

FIG. 2: Spin density distribution in the A, B and C condensate phases. Left, the isosurface of the spin density (red-positive, blue-negative) in the A-phase of ideal cubic structure obtained with Wien2k. Right, detail of the spin density distributions around the Co atom in the A, B and C states. For the collinear (A, B) distribution we show the positive and negative isosurfaces of the spin projection. For the non-collinear (C) distribution we show the spin distribution of the $x^4+y^4+z^4 = \text{const}$ surface where the normal component vanishes.

A. Cubic structure without spin-orbit coupling

Three distinct ordered states referred to as A, B and C were found to be stable for the cubic system without SOC. The A-type states are described by the order parameter[38]

$$\boldsymbol{\phi}^{(A)}_k = (-1)^k\begin{pmatrix}0&0&\lambda'\\0&0&0\\0&0&0\end{pmatrix} \equiv (-1)^k\begin{pmatrix}\boldsymbol{\eta}\\0\\0\end{pmatrix} \quad (5)$$

with real λ' and $(-1)^k$ indicating opposite sign on the two sublattices. While there are no ordered spin moments (dipoles) in this state, there is a finite local spin density (see Fig. 2) around Co atoms, which lead Halperin and Rice[34] to introduce the name spin-density wave (SDW) condensate. Applying Hamiltonian symmetries one can generate all possible states belonging to the A-phase. In a general form, the A-type order parameter has two rows of zeros and one

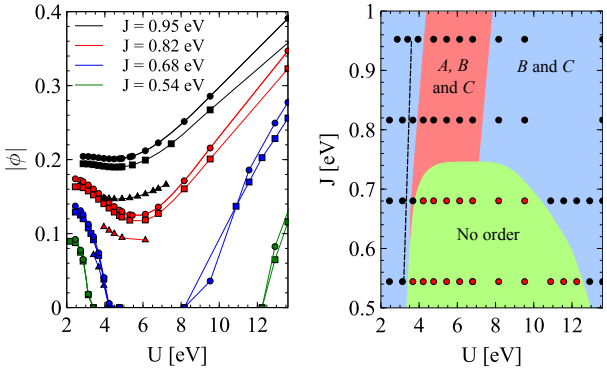

FIG. 3: (Left) The order parameter $|\phi|$ vs U for various J values. The A, B and C phases are represented with triangles, squares and circles. (Right) The U-J phase diagram indicating the local stability of the three excitonic phases. The circles mark the points where actual calculations were performed. The dashed line shows where the gap opens in the normal phase.

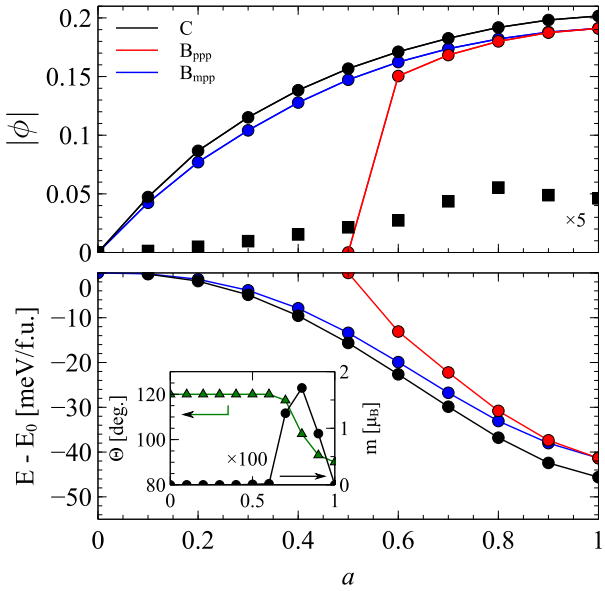

FIG. 4: (Upper panel) The evolution of the staggered real $|\phi'|$ (circles) and uniform imaginary $|\phi''|$ (squares) components of the order parameter along the path between the cubic ($a = 1$) and experimental ($a = 0$) $LaCoO_3$ structures in the C, B_{mpp} and B_{ppp} phases. (Bottom panel) The condensation energy - the difference between the total energy of ordered and normal solution for the three stable solutions. In the inset we show the evolution of the ordered (ferromagnetic) moments on Co sites and the angle Θ between the spin vectors $\boldsymbol{\eta}_\beta$ and $\boldsymbol{\eta}_{\beta'}$ in different orbital channels in the C phase. The results were obtained with U=3.90 eV and J=0.95 eV.

row with real vector of the length $|\boldsymbol{\eta}| = \lambda'$. We have repeated calculations with condensate in each of the three orbital channels ($\hat{x}$, $\hat{y}$, $\hat{z}$) as well as several general orientations of the spin-vector $\boldsymbol{\eta}$ to verify that these solutions are connected by the corresponding symmetry operations and lead to the same total energies. Given the difference of Γ_α matrices this is a numerically nontrivial test.

In the B-type state the condensate is distributed equally among all orbital channels. Similar to the A-type the order parameter is real and staggered

$$\boldsymbol{\phi}_k^{(B)} = (-1)^k \begin{pmatrix} 0 & 0 & \lambda' \\ 0 & 0 & \lambda' \\ 0 & 0 & \lambda' \end{pmatrix} \equiv (-1)^k \begin{pmatrix} \boldsymbol{\eta}_{\hat{x}} \\ \boldsymbol{\eta}_{\hat{y}} \\ \boldsymbol{\eta}_{\hat{z}} \end{pmatrix}. \quad (6)$$

The spin density in this phase, shown in Fig. 2, is collinear and gives rise to no ordered dipole. In the general form, the B-type order parameter consists real row vectors of equal length that are mutually parallel or anti-parallel, $\pm\boldsymbol{\eta}_{\hat{x}} = \pm\boldsymbol{\eta}_{\hat{y}} = \pm\boldsymbol{\eta}_{\hat{z}}$.

The C-type states have the most complicated structure. Similar to the B-type the condensate has equal weight in all orbital channels, but the corresponding spin vectors $\boldsymbol{\eta}_\alpha$ are mutually orthogonal. The dominant part of the ϕ is staggered and real, but there is a small uniform and imaginary component, which has the same matrix structure as the staggered part

$$\boldsymbol{\phi}_k^{(C)} = (-1)^k \begin{pmatrix} \lambda' & 0 & 0 \\ 0 & \lambda' & 0 \\ 0 & 0 & \lambda' \end{pmatrix} + i \begin{pmatrix} \lambda'' & 0 & 0 \\ 0 & \lambda'' & 0 \\ 0 & 0 & \lambda'' \end{pmatrix}. \quad (7)$$

There is a complicated non-collinear distribution of spin density, shown in Fig. 2, which does not give rise to an ordered dipole. The general form of the $\boldsymbol{\phi}_k^{(C)}$ is $(-1)^k\lambda' + i\lambda''$ times and an $O(3)$ matrix, where the $SO(3)$ part comes from the action of spin rotations on $\boldsymbol{\phi}_k^{(C)}$ of Eq. 7 and $-\boldsymbol{\phi}_k^{(C)}$ is obtained by time reversal. The O_h orbital symmetry does not add additional degenerate states in this case.

For all studied values of the interaction parameters of U and J we found the C-phase to have the lowest energy among the stable ordered solutions. In

EC phase	$\|\boldsymbol{\phi}'\|$	$\|\boldsymbol{\phi}''\|$	$E - E_0[meV/f.u.]$
A-phase	0.151	0.000	-13.32
B-phase	0.191	0.000	-20.39
C-phase	0.202	0.009	-22.81

TABLE I: The amplitudes of the staggered real $|\boldsymbol{\phi}'|$ and uniform imaginary $|\boldsymbol{\phi}''|$ components of the order parameter together with the condensation energies for the LDA+U solutions (U=3.90 eV, J=0.95 eV) in the cubic structure.

Table I we compare the condensation energies (the difference between the total energy of the ordered and normal state) for $U = 3.95$ eV and $J = 0.95$ eV.

Stability of the excitonic condensate as a function of the interaction parameters is summarised in Fig. 3. We find that ordered solutions exist on the small U side where the normal state is metallic as well as for large U where the normal state has a well developed gap. At intermediate U values we observed reduction of the order parameter $\boldsymbol{\phi}$ for larger J values and complete suppression of the ordered state for smaller J's. This behavior is likely related to the crossover from weak coupling regime, where the transition involves mostly states close to the Fermi surface, to the strong-coupling regime, where the transition involves states in the entire Brillouin zone. We find that the A-phase exists as a metastable solution only at intermediate U and large J. Outside this region the A-like states converge to either B or C solutions. The results in Fig. 3 allow for two general conclusions. Larger J favors excitonic condensation, most likely by bringing the excited IS states energetically closer the LS ground state. More stable state have larger order parameter $|\phi|$.

B. Real $LaCoO_3$ structure without spin-orbit coupling

The actual structure of $LaCoO_3$ differs from the ideal cubic perovskite by a rhombohedral distortion. The crystal expands and the CoO_6 octahedra rotate along one of the cubic body diagonals. In the following we study the impact of this structural modification on the excitonic phase. To this end we fix the interaction parameters at U= 3.90 eV and J=0.95 eV and construct several structures that continuously interpolate between the atomic positions of the cubic $\mathbf{r}_{cubic}$ and the real $\mathbf{r}_{real}$ structure

$$\mathbf{r} = a\mathbf{r}_{cubic} + (1-a)\mathbf{r}_{real}. \tag{8}$$

Upon lifting the cubic symmetry the anomalous part of the Co-3d occupation matrix slightly deviates from (4), nevertheless, $\boldsymbol{\phi}$ can still be used as an order parameter. In Fig. 4 we show the evolution of the B and C phases with the distortion a. The distortion suppresses the excitonic LRO - no ordered solution is found for the actual $LaCoO_3$ structure. For all a values the C-phase retains the lowest energy among the stable states with LRO.

There are several more subtle observations. Eliminating some of the orbital symmetries splits the B-type states into two distinct sets depending on the signs of $\boldsymbol{\eta}_\alpha$: $B_{\rm ppp}$ connected to $+++$ state and $B_{\rm mpp}$ connected to $-++$ state. The latter is found to be more stable. The $\boldsymbol{\phi}^{(B)}$ remains purely real for all studied structures and with no ordered spin dipoles.

There is no branching of the C solutions since they all can be connected by spin rotations or time reversal. The uniform imaginary part of $\boldsymbol{\phi}^{(C)}$ is suppressed faster than the staggered real part. The angle Θ between the spin-vectors $\boldsymbol{\eta}_\alpha$ (we consider only the dominant real part of $\boldsymbol{\phi}^{(C)}$) varies from 90$^{\rm o}$ to 120$^{\rm o}$, where it saturates for $a \simeq 0.6$. For the states with Θ between these two limits we observe a small ferromagnetic polarization m. These observations are summarised in Fig. 4.

C. Spin-orbit coupling

The SOC breaks the spin-rotational symmetry and introduces coupling within the t_{2g} subshell as well as between the e_g and t_{2g} orbitals. The latter can be viewed in the present context as a source field generating $\phi^{(\rm SOC)}_{\alpha\beta} = i\lambda\delta_{\alpha\beta}$. This raises several questions. Does excitonic LRO survive in the presence of SOC, i.e., is there a symmetry distinction between the normal and ordered phase? How does does SOC interact with the excitonic condensate?

We have performed calculations (U=3.90 eV, J=0.95 eV) in the cubic structure starting from several initial conditions, corresponding to the normal state and B and C-type LROs. In all cases the calculations converged to two distinct, but symmetry

Structure	$\|\boldsymbol{\phi}'\|$	$\|\boldsymbol{\phi}''\|$	$E - E_0$[meV/f.u.]
cubic, no SOC	0.202	0.009	-22.81
cubic with SOC	0.197	0.095	-25.36
real with SOC	0.014	0.090	-0.03

TABLE II: The amplitudes of the staggered real $|\boldsymbol{\phi}'|$ and uniform imaginary $|\boldsymbol{\phi}''|$ components of the order parameter together with the condensation energies for the LDA+U solutions (U=3.90 eV, J=0.95 eV). We compare the cubic structure (C-phase) with and without SOC and show the result for real $LaCoO_3$ structure with SOC (there is no ordered solution in real structure without SOC).

related, selfconsistent states[39]

$$\boldsymbol{\phi}_k = (-1)^k \begin{pmatrix} -0.12 & 0.00 & 0.00 \\ 0.00 & 0.06 & 0.09 \\ 0.00 & -0.09 & -0.06 \end{pmatrix} + i \begin{pmatrix} 0.06 & 0.00 & 0.00 \\ 0.00 & 0.06 & 0.00 \\ 0.00 & 0.00 & 0.06 \end{pmatrix}. \quad (9)$$

The uniform imaginary part is essentially the same as in the normal state, i.e., it is generated by SOC and does not represent a spontaneous symmetry breaking. Finite real part $\boldsymbol{\phi}'$, however, breaks the time-reversal symmetry and thus distinguishes the ordered and the normal states. Naively, one might have expected that SOC selects one out of the continuum of degenerate C-type states (7) by locking the $\boldsymbol{\eta}_\alpha$ spin-vectors to specific crystallographic directions without changing their relative magnitudes and angles. The solution, shown in (9), is more complicated and the ordered state exhibits no residual symmetry. The ordered spin moment per Co in (9) is less than 0.001 μ_B .

Comparing the condensation energies in the cases with and without SOC (see Table II) we find that SOC promotes the condensation. Indeed, with SOC we found a marginally stable ordered solution also in the real $LaCoO_3$ structure where it did not exist without SOC.

IV. DISCUSSION

To understand the behavior and stability of different excitonic phases is difficult and the all electron scheme, such as the Wien2k LDA+U used so far, is too complex for this purpose. Therefore we resort to a simplified model below. Before we do that let us summarize the main trends observed in the numerical results: i) there is a preference for real staggered order, ii) condensate distributed among the orbital channels is more stable, iii) rhombohedral distortion suppresses the condensation, iv) small imaginary uniform component of the order parameter appears in some phases, v) the uniform component is suppressed fast than the staggered one by rhombohedral distortion, vi) the spin-orbit coupling favors formation of the condensate.

To discuss these features in a comprehensible way we use an effective low energy model that lives in a Hilbert space spanned by LS, IS and HS multiplets on each Co site. A further simplification can be achieved in that we view the LS lattice as a vacuum state, IS state as an exciton[22] created by the bosonic operator $d^\dagger_{i\alpha\beta}$ with i, $\alpha = \hat{x}, \hat{y}, \hat{z}$ and $\beta = x, y, z$ being the site, orbital channel and spin index, respectively. The HS state can be viewed as a bi-exciton consisting of two excitons with different orbital characters.[40] The resulting model is a generalized version of the strong coupling model of Refs. 32,33.

$$H = \epsilon \sum_{i\alpha\beta} d^\dagger_{i\alpha\beta} d_{i\alpha\beta} + \sum_{ij\alpha\beta} t_{ij}(\alpha) d^\dagger_{i\alpha\beta} d_{j\alpha\beta} + \frac{1}{2} \sum_{ij\alpha\beta} \bar{t}_{ij}(\alpha)(d^\dagger_{i\alpha\beta} d^\dagger_{j\alpha\beta} + h.c.) + H_3 + H_4. \quad (10)$$

Hard core constraint of maximum one boson in a given orbital channel is assumed. The terms H_3 and H_4 contain three and four d operators respectively and have a complicated form. The order parameter $\boldsymbol{\phi}$ on a given site is simply the expectation value $\phi_{\alpha\beta} = \langle d_{\alpha\beta} \rangle$.

i) The preference for real staggered order is related to the positive signs of $t_{ij}(\alpha), \bar{t}_{ij}(\alpha) > 0$ in (10) as can be seen by replacing the d operators with their expectation values. The t-term favors staggered order irrespective of whether $\boldsymbol{\phi}$ is real or imaginary. The $\bar{t}$-term is minimized by both staggered real and uniform imaginary $\boldsymbol{\phi}$. The staggered real order therefore mininizes both terms simultaneously. Positive $t_{ij}(\alpha)$ is a general feature of the perovskite structure arising from the relevant $t_{2g} \leftrightarrow t_{2g}$ and $e_g \leftrightarrow e_g$ nearest-neighbor hoppings having the same (negative) signs.[2] The $\bar{t}$-terms originate from intersite cross-hopping between $t_{2g} \leftrightarrow e_g$ orbitals and the pair-hopping part of the on-site interaction.[2,32,35]

Since the relevant cross-hoppings between nearest and next nearest neighbors in the cubic structure are forbidden by symmetry we are left with pair-hopping which yields $\bar{t}_{ij}(\alpha) > 0$.[2]

ii) In the mean-field approximation the bilinear part of (10) has a high $O(9)$ symmetry (upon summation over the nearest neighbors). The matrix form of the order parameter $\boldsymbol{\phi}$ is thus determined by the H_3 and H_4 terms. The discussion of all symmetry allowed H_3 and H_4 terms is beyond the scope of this paper. We point out that already in the case of single orbital flavor[33] there are several contributions describing the inter-site repulsion and spin-exchange between the bosons. Without detailed knowledge of the model parameters the following discussion is necessarily speculative. We propose the nearest-neighbor d-d repulsion to favor the distribution of condensate among the orbital channels. We argue that the d-d repulsion between the d-bosons of the same orbital flavor is substantially stronger than inter-flavor repulsion. If so, a condensate distributed among as many channels as possible generates less positive interaction energy than a condensate concentrated in a single channel.

The difference between inter- and intra-channel repulsion can be understood as follows. A single exciton can lower its energy by virtual hopping to the empty neighbor sites. These processes are Pauli-blocked (hard-core constraint in Eq. 10) when neighbors are occupied by excitons of the same orbital flavor, resulting in d-d repulsion. The virtual hopping is modified, but not blocked, by an exciton with different orbital flavor and thus the repulsion is weaker in this case.[41]

iii) Suppression of the excitonic order by rhombohedral distortion may be a simple consequence of reduced hopping due to the Co-O-Co bond bending. Since we do not have a detailed understanding of the detailed balance between the hopping channels that are reduced and those that are opened due to the distortion, we leave this as a numerical observation.

The remaining points are discussed in the following section.

A. Uniform imaginary order

To understand the origin of the uniform component of the order parameter would require detailed knowledge of the parameters in (10). Possibility of detailed quantitative mapping of the LDA+U results on model (10) is questionable and we do not have such ambition. We only demonstrate a possible mechanism to obtain a finite uniform component and discuss its general features. To this end we drop the orbital degeneracy of (10) and use a specific form of H_4, corresponding to spin-spin exchange[33]

$$\begin{aligned} H' =& \epsilon \sum_i \mathbf{d}_i^\dagger \cdot \mathbf{d}_i + t \sum_{\langle ij \rangle} (\mathbf{d}_i^\dagger \cdot \mathbf{d}_j + h.c.) \\ &+ \bar{t} \sum_{\langle ij \rangle} (\mathbf{d}_i^\dagger \cdot \mathbf{d}_j^\dagger + h.c.) - J \sum_{\langle ij \rangle} (\mathbf{d}_i^\dagger \wedge \mathbf{d}_i) \cdot (\mathbf{d}_j^\dagger \wedge \mathbf{d}_j). \end{aligned} \tag{11}$$

We will use the variational ground state with staggered real and uniform imaginary, mutually orthogonal, components of the condensate

$$|\Psi\rangle = \prod_k (s|0\rangle_k + (-1)^k x|x\rangle_k + iy|y\rangle_k) \tag{12}$$

with the normalisation $s^2 + x^2 + y^2 = 1$. The variational energy per lattice site is

$$\begin{aligned} &\langle \Psi | H' | \Psi \rangle / N = \epsilon(x^2 + y^2) \\ &- Z(\bar{t} + t)x^2(1 - x^2) - Z(\bar{t} - t)y^2(1 - y^2) \\ &+ 2Zx^2y^2(\bar{t} - J), \end{aligned} \tag{13}$$

where Z is the number of nearest neighbors. Expression (13) is then minimized subject to the conditions $x^2 > 0$, $y^2 > 0$ and $x^2 + y^2 \leq 1$.

Let us consider separately the effect of each inter-site term. Both t and $\bar{t}$ terms contribute to the condensation characterised by finite $|\phi|^2 = (1 - x^2 - y^2)(x^2 + y^2)$. The positive hopping $t > 0$ contribution is minimized by staggered order irrespective of the complex phase of ϕ, i.e. $y = 0$ in (13). The positive pair creation $\bar{t} > 0$ term has degenerate minima for staggered real or uniform imaginary ϕ, i.e. solutions with the same $x^2 + y^2$ are degenerate. The antiferromagnetic exchange term $J > 0$ favors states with equal $x^2 = y^2$. The ratio y/x is thus determined by the balance between the hopping t and exchange J.

Tuning the system from pure LS state ($x^2 + y^2 = 0$), e.g. by varying ϵ, we first obtain the staggered condensate and only at larger values of $x^2 + y^2$ the uniform component possibly appears. This is because t contributes to (13) in the second order while J only in the forth order.

Let us discuss the relevance of the present toy model to the studied material. The hopping t and pair creation $\bar{t}$ terms in (10) are diagonal in orbital indices which can justify the reduction to a single orbital flavor. On the other hand the exchange term is certainly not the only force driving the appearance of the uniform order parameter. Should it be so, uniform $\boldsymbol{\phi}''$ would have appeared also in the A and B phases. The uniform $\boldsymbol{\phi}''$ appearing only in the C phase, indicates that the forth order term in the real material has a more complicated structure combining several orbital flavors.

Nevertheless, the present toy model shows how the imaginary uniform component $\boldsymbol{\phi}''$ of the order parameter can appear. Its origin in a 4th order term explains why it disappears faster than the real staggered component $\boldsymbol{\phi}'$, as shown in Fig. 4. Finally, spontaneous appearance of uniform $\boldsymbol{\phi}''$ explains the stabilising effect of SOC. The simultaneous presence of uniform $\boldsymbol{\phi}''$ and staggered $\boldsymbol{\phi}'$ generates a negative $(H_3 + H_4)$ contribution to the energy of the ordered state, while the $\boldsymbol{\phi}''$ alone generates a positive contribution proportional to t. Without SOC, both of these terms contribute to the condensation energy and partially cancel each other out. With SOC, roughly the same $\boldsymbol{\phi}''$ appears in the normal and the ordered phases and thus the above positive t-proportional term does not contribute to the condensation energy.

V. CONCLUSIONS

We have used the LDA+U approach to investigate excitonic magnetism in prototypical cubic perovskite with the d^6 configuration of transition metal ion as well as in the real structure of $LaCoO_3$. We found that stable excitonic solutions exist for realistic interaction parameters. Among the possible ordered states there is a preference for equal distribution of the condensate among the orbital and spin channels. The rhombohedral distortion of the real $LaCoO_3$ structure is detrimental to the exciton condensation, while the spin-orbit coupling is favorable for the transition. Given the absence of the experimentally observed phase transitions in $LaCoO_3$, our results suggest that the material is close to the excitonic instability and suggest ways how the instability can be approached.

Acknowledgments

We thank A. Sotnikov, A. Kauch and A. Hariki for discussions. This work has received funding from the European Research Council (ERC) under the European Union's Horizon 2020 research and innovation programme (grant agreement No 646807).

VI. APPENDIX

The relationship between the cubic and spherical harmonics:

$$\begin{aligned} d_{xy} &= \frac{i}{\sqrt{2}}\left(Y^2_{-2} - Y^2_2\right) \\ d_{xz} &= \frac{1}{\sqrt{2}}\left(Y^2_{-1} - Y^2_1\right) \\ d_{yz} &= \frac{i}{\sqrt{2}}\left(-Y^2_{-1} - Y^2_1\right) \\ d_{x^2-y^2} &= \frac{1}{\sqrt{2}}\left(Y^2_{-2} + Y^2_2\right) \\ d_{3z^2-r^2} &= Y^2_0 \end{aligned} \tag{14}$$

The $d_{z^2-x^2}$ and $d_{y^2-z^2}$ orbitals in the above cubic harmonic basis.

$$\begin{aligned} d_{z^2-x^2} &= \frac{1}{2}\left(\sqrt{3}d_{3z^2-r^2} - d_{x^2-y^2}\right) \\ d_{y^2-z^2} &= \frac{1}{2}\left(\sqrt{3}d_{3z^2-r^2} + d_{x^2-y^2}\right) \end{aligned} \tag{15}$$

The Γ_α matrices (2) in the $\{d_{xy},\ d_{xz},\ d_{yz},\ d_{x^2-y^2},\ d_{3z^2-r^2}\}$ basis of cubic harmonics:

$$\Gamma'_{\hat{x}} = \frac{1}{2}\begin{pmatrix} 0 & 0 & 0 & 0 & 0 \\ 0 & 0 & 0 & 0 & 0 \\ 0 & 0 & 0 & -1 & -\sqrt{3} \\ 0 & 0 & -1 & 0 & 0 \\ 0 & 0 & -\sqrt{3} & 0 & 0 \end{pmatrix}$$

$$\Gamma'_{\hat{y}} = \frac{1}{2}\begin{pmatrix} 0 & 0 & 0 & 0 & 0 \\ 0 & 0 & 0 & -1 & \sqrt{3} \\ 0 & 0 & 0 & 0 & 0 \\ 0 & -1 & 0 & 0 & 0 \\ 0 & \sqrt{3} & 0 & 0 & 0 \end{pmatrix}$$

$$\Gamma'_{\hat{z}} = \begin{pmatrix} 0 & 0 & 0 & 1 & 0 \\ 0 & 0 & 0 & 0 & 0 \\ 0 & 0 & 0 & 0 & 0 \\ 1 & 0 & 0 & 0 & 0 \\ 0 & 0 & 0 & 0 & 0 \end{pmatrix}$$

$$\Gamma''_{\hat{x}} = \frac{i}{2}\begin{pmatrix} 0 & 0 & 0 & 0 & 0 \\ 0 & 0 & 0 & 0 & 0 \\ 0 & 0 & 0 & -1 & -\sqrt{3} \\ 0 & 0 & 1 & 0 & 0 \\ 0 & 0 & \sqrt{3} & 0 & 0 \end{pmatrix}$$

$$\Gamma''_{\hat{y}} = \frac{i}{2}\begin{pmatrix} 0 & 0 & 0 & 0 & 0 \\ 0 & 0 & 0 & -1 & \sqrt{3} \\ 0 & 0 & 0 & 0 & 0 \\ 0 & 1 & 0 & 0 & 0 \\ 0 & -\sqrt{3} & 0 & 0 & 0 \end{pmatrix}$$

$$\Gamma''_{\hat{z}} = i\begin{pmatrix} 0 & 0 & 0 & 1 & 0 \\ 0 & 0 & 0 & 0 & 0 \\ 0 & 0 & 0 & 0 & 0 \\ -1 & 0 & 0 & 0 & 0 \\ 0 & 0 & 0 & 0 & 0 \end{pmatrix} \tag{16}$$

The Γ_α matrices (2) in the $\{Y_2,\ Y_1,\ Y_0,\ Y_{-1},\ Y_{-2}\}$ basis of spherical harmonics:

$$\Gamma'_{\hat{x}} = \frac{i}{4}\begin{pmatrix} 0 & -1 & 0 & -1 & 0 \\ 1 & 0 & \sqrt{6} & 0 & 1 \\ 0 & -\sqrt{6} & 0 & -\sqrt{6} & 0 \\ 1 & 0 & \sqrt{6} & 0 & 1 \\ 0 & -1 & 0 & -1 & 0 \end{pmatrix}$$

$$\Gamma'_{\hat{y}} = \frac{1}{4}\begin{pmatrix} 0 & 1 & 0 & -1 & 0 \\ 1 & 0 & -\sqrt{6} & 0 & 1 \\ 0 & -\sqrt{6} & 0 & \sqrt{6} & 0 \\ -1 & 0 & \sqrt{6} & 0 & -1 \\ 0 & 1 & 0 & -1 & 0 \end{pmatrix}$$

$$\Gamma'_{\hat{z}} = i\begin{pmatrix} 0 & 0 & 0 & 0 & -1 \\ 0 & 0 & 0 & 0 & 0 \\ 0 & 0 & 0 & 0 & 0 \\ 0 & 0 & 0 & 0 & 0 \\ 1 & 0 & 0 & 0 & 0 \end{pmatrix}$$

$$\Gamma''_{\hat{x}} = -\frac{1}{4}\begin{pmatrix} 0 & 1 & 0 & 1 & 0 \\ 1 & 0 & \sqrt{6} & 0 & 1 \\ 0 & \sqrt{6} & 0 & \sqrt{6} & 0 \\ 1 & 0 & \sqrt{6} & 0 & 1 \\ 0 & 1 & 0 & 1 & 0 \end{pmatrix}$$

$$\Gamma''_{\hat{y}} = \frac{i}{4}\begin{pmatrix} 0 & -1 & 0 & 1 & 0 \\ 1 & 0 & -\sqrt{6} & 0 & 1 \\ 0 & \sqrt{6} & 0 & -\sqrt{6} & 0 \\ -1 & 0 & \sqrt{6} & 0 & -1 \\ 0 & -1 & 0 & 1 & 0 \end{pmatrix}$$

$$\Gamma''_{\hat{z}} = \begin{pmatrix} -1 & 0 & 0 & 0 & 0 \\ 0 & 0 & 0 & 0 & 0 \\ 0 & 0 & 0 & 0 & 0 \\ 0 & 0 & 0 & 0 & 0 \\ 0 & 0 & 0 & 0 & 1 \end{pmatrix} \tag{17}$$

* Electronic address: kunes@ifp.tuwien.ac.at

1 G. Khaliullin, Phys. Rev. Lett. **111**, 197201 (2013).
2 J. Kuneš and P. Augustinský, Phys. Rev. B **89**, 115134 (2014).
3 J. Kuneš and P. Augustinský, Phys. Rev. B **90**, 235112 (2014).
4 T. Kaneko and Y. Ohta, Phys. Rev. B **90**, 245144 (2014).
5 T. Kaneko, B. Zenker, H. Fehske, and Y. Ohta, Phys. Rev. B **92**, 115106 (2015).
6 J. Chaloupka and G. Khaliullin, Phys. Rev. Lett. **116**, 017203 (2016).
7 A. Jain, M. Krautloher, J. Porras, G. H. Ryu, D. P. Chen, D. L. Abernathy, J. T. Park, A. Ivanov, J. Chaloupka, G. Khaliullin, et al., arXiv:1510.07011.
8 R. A. Bari and J. Sivardière, Phys. Rev. B **5**, 4466 (1972).
9 K. Knížek, Z. Jirák, J. Hejtmánek, P. Novák, and W. Ku, Phys. Rev. B **79**, 014430 (2009).
10 J. Kuneš and V. Křápek, Phys. Rev. Lett. **106**, 256401 (2011).
11 M. A. Korotin, S. Y. Ezhov, I. V. Solovyev, V. I. Anisimov, D. I. Khomskii, and G. A. Sawatzky, Phys. Rev. B **54**, 5309 (1996).

[12] S. Yamaguchi, Y. Okimoto, and Y. Tokura, Phys. Rev. B **55**, R8666 (1997).
[13] Y. Tokura, Y. Okimoto, S. Yamaguchi, H. Taniguchi, T. Kimura, and H. Takagi, Phys. Rev. B **58**, R1699 (1998).
[14] G. Zhang, E. Gorelov, E. Koch, and E. Pavarini, Phys. Rev. B **86**, 184413 (2012).
[15] P. G. Radaelli and S.-W. Cheong, Phys. Rev. B **66**, 094408 (2002).
[16] G. Maris, Y. Ren, V. Volotchaev, C. Zobel, T. Lorenz, and T. T. M. Palstra, Phys. Rev. B **67**, 224423 (2003).
[17] S. K. Pandey, S. Khalid, N. P. Lalla, and A. V. Pimpale, Journal of Physics: Condensed Matter **18**, 10617 (2006).
[18] V. V. Sikolenko, I. O. Troyanchuk, V. V. Efimov, E. A. Efimova, S. I. Tiutiunnikov, D. V. Karpinsky, S. Pascarelli, O. Zaharko, A. Ignatov, D. Aquilanti, et al., Journal of Physics: Conference Series **712**, 012118 (2016).
[19] M. M. Altarawneh, G.-W. Chern, N. Harrison, C. D. Batista, A. Uchida, M. Jaime, D. G. Rickel, S. A. Crooker, C. H. Mielke, J. B. Betts, et al., Phys. Rev. Lett. **109**, 037201 (2012).
[20] M. Rotter, Z.-S. Wang, A. T. Boothroyd, D. Prabhakaran, A. Tanaka, and M. Doerr, Scientific Reports **4**, 7003 EP (2014), article.
[21] A. Ikeda, T. Nomura, Y. H. Matsuda, A. Matsuo, K. Kindo, and K. Sato, Phys. Rev. B **93**, 220401 (2016).
[22] A. Sotnikov and J. Kuneš, Sci. Rep. **6**, 30510 (2016).
[23] S. Tsubouchi, T. Kyômen, M. Itoh, P. Ganguly, M. Oguni, Y. Shimojo, Y. Morii, and Y. Ishii, Phys. Rev. B **66**, 052418 (2002).
[24] J. Hejtmánek, E. Šantavá, K. Knížek, M. Maryško, Z. Jirák, T. Naito, H. Sasaki, and H. Fujishiro, Phys. Rev. B **82**, 165107 (2010).
[25] K. Knížek, J. Hejtmánek, M. Maryško, P. Novák, E. Šantavá, Z. Jirák, T. Naito, H. Fujishiro, and C. de la Cruz, Phys. Rev. B **88**, 224412 (2013).
[26] A. Ikeda, S. Lee, T. T. Terashima, Y. H. Matsuda, M. Tokunaga, and T. Naito, Phys. Rev. B **94**, 115129 (2016).
[27] J. Nasu, T. Watanabe, M. Naka, and S. Ishihara, Phys. Rev. B **93**, 205136 (2016).
[28] T. Tatsuno, E. Mizoguchi, J. Nasu, M. Naka, and S. Ishihara, Journal of the Physical Society of Japan **85**, 083706 (2016).
[29] V. I. Anisimov, J. Zaanen, and O. K. Andersen, Phys. Rev. B **44**, 943 (1991).
[30] A. I. Liechtenstein, V. I. Anisimov, and J. Zaanen, Phys. Rev. B **52**, R5467 (1995).
[31] P. Blaha, K. Schwarz, G. K. H. Madsen, D. Kvasnicka, and J. Luitz, *WIEN2k, An Augmented Plane Wave + Local Orbitals Program for Calculating Crystal Properties* (Technische Universität Wien, Austria, 2001).
[32] L. Balents, Phys. Rev. B **62**, 2346 (2000).
[33] J. Kuneš, J. Phys.: Condens. Matter **27**, 333201 (2015).
[34] B. I. Halperin and T. M. Rice, *Solid State Physics* (Academic Press, New York, 1968), vol. 21, p. 115.
[35] J. Kuneš and D. Geffroy, Phys. Rev. Lett. **116**, 256403 (2016).
[36] from Ref. 15 at 5 K
[37] Rotation of the spin coordinates required small modification of the LAPWDM code from Wien2k package.
[38] This describes one of the set of degenerate states related by the symmetries of the Hamiltonian.
[39] Note that with SOC the symmetry operations must be applied to spin (rows) and orbital (columns) indices simultaneously.
[40] Here we ignore the fact that while $|\langle IS_{\hat{x}}|d^\dagger_{\hat{x}}|LS\rangle| = 1$, adding a second exciton, e.g., $|\langle HS_{\hat{z}}|d^\dagger_{\hat{y}}|IS_{\hat{x}}\rangle| \simeq \frac{\sqrt{3}}{2}$, has a weight less than one. This is because only the hole t_{2g}, but not the electron e_g, components of excitons in different orbital channels are mutually orthogonal.
[41] An inter-site attraction between different orbital flavors is possible in principle.